ACS Chemical Neuroscience

Research Article

pubs.acs.org/chemneuro

Dendritic Polyglycerol Sulfates in the Prevention of Synaptic Loss and Mechanism of Action on Glia

Dusica Maysinger,*[,†] Jeff Ji,[†] Alexandre Moquin,[†] Shireen Hossain,[†] Mark A. Hancock,[†] Issan Zhang,[†] Philip K.Y. Chang,[†] Matthew Rigby,[‡] Madeleine Anthonisen,[‡] Peter Grütter,[‡] John Breitner,[§] R. Anne McKinney,[†] Sabine Reimann,[∥] Rainer Haag,[∥] and Gerhard Multhaup[†]

[†]Department of Pharmacology and Therapeutics, McGill University, Montreal, Canada H3G 1Y6

[‡]Department of Physics, McGill University, Montreal, Canada H3A 2T8

[§]Douglas Hospital Research Centre, McGill University, Montreal, Canada H4H 1R3

[∥]Institut für Chemie und Biochemie, Freie Universität Berlin, 14195 Berlin, Germany

Supporting Information

ABSTRACT: Dendritic polyglycerols (dPG), particularly dendritic polyglycerol sulfates (dPGS), have been intensively studied due to their intrinsic anti-inflammatory activity. As related to brain pathologies involving neuroinflammation, the current study examined if dPG and dPGS can (i) regulate neuroglial activation, and (ii) normalize the morphology and function of excitatory postsynaptic dendritic spines adversely affected by the neurotoxic 42 amino acid amyloid-β ($A\beta_{42}$) peptide of Alzheimer disease (AD). The exact role of neuroglia, such as microglia and astrocytes, remains controversial especially their positive and negative impact on inflammatory processes in AD. To test dPGS effectiveness in AD models we used primary neuroglia and organotypic hippocampal slice cultures exposed to $A\beta_{42}$ peptide. Overall, our data indicate that dPGS is taken up by both microglia and astrocytes in a concentration- and time-dependent manner. The mechanism of action of dPGS involves binding to $A\beta_{42}$, i.e., a direct interaction between dPGS and $A\beta_{42}$ species interfered with $A\beta$ fibril formation and reduced the production of the neuroinflammagen lipocalin-2 (LCN2) mainly in astrocytes. Moreover, dPGS normalized the impairment of neuroglia and prevented the loss of dendritic spines at excitatory synapses in the hippocampus. In summary, dPGS has desirable therapeutic properties that may help reduce amyloid-induced neuroinflammation and neurotoxicity in AD.

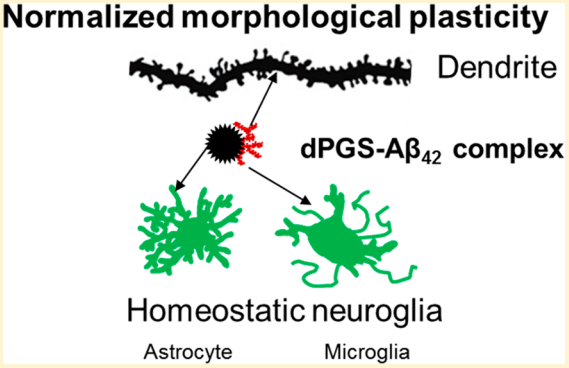

KEYWORDS: *Dendritic polyglycerol sulfates, amyloid beta, dendritic spines, astrocytes, microglia, LCN-2*

INTRODUCTION

Many neurodegenerative disorders, including Alzheimer disease (AD), are characterized by alterations in both astrocytes and microglia activation states that reflect underlying changes in the brain's innate immune system. Innate immune signaling is thought to be not only altered in the early stages of AD, but is also skewed toward an activated state during aging of the brain in the absence of a triggering proteinopathy.[1,2] The self-assembly of monomeric amyloidogenic proteins into oligomeric species and their subsequent conversion into fibrils, is a pathological hallmark of neurological disorders including AD.[3] Both microglia and astrocytes are key players in the clearance of protein aggregates, either by binding and phagocytosis of protein aggregates or by attracting and activating nearby glial cells.[4,5] Proinflammatory cytokines including IL-1 and IL-6 stimulate gliosis, thereby enhancing $A\beta$ phagocytosis in transgenic mice.[6] Phagocytic processes and the elimination of internalized materials through lysosomal degradation are dysregulated in aging.[7] With increasing age, amyloid transitions from nontoxic monomers to toxic oligomers, ultimately leading to the deterioration of neural circuitries.[8] Emerging literature suggests that "mild" activation of neuroglia for a limited time could be beneficial since it facilitates microglia-mediated $A\beta$ clearance from the brain. If microglia are chronically or hyper activated, however, they can turn astrocytes into reactive, cytotoxic astrocytes (A1).[9] Indeed, A1/C3-positive reactive astrocytes, which do not support neuronal functions, were detected in AD postmortem brains.[9] A single-cell RNA-sequencing in immune cells isolated from mouse models with familiar AD mutations revealed subpopulations of microglia named "disease-associated microglia" and "homeostatic microglia".[10] These studies suggest a progression of microglia transformation from homeostatic to diseased-associated microglia in AD.

Received: August 4, 2017
Accepted: October 27, 2017
Published: October 27, 2017

DOI: 10.1021/acschemneuro.7b00301
ACS Chem. Neurosci. 2018, 9, 260−271

Epidemiological studies have suggested long-term treatment with nonsteroidal anti-inflammatory drugs (NSAIDs) can confer protection, but clinical trials with celecoxib- and naproxen-treated AD patients did not show any significant improvements.[11] Several studies suggest that treatment effects with NSAIDS could vary depending on underlying clinically silent AD pathology and initiation of NSAID therapy.[12−17]

Recent studies have shown that a small NSAID, called sulindac sulfide, can reduce Aβ toxicity by altering the kinetics of fibril formation.[18] Likewise, we have previously shown that an Aβ_{42}-oligomer Interacting Peptide (AIP) can interact with low-order Aβ_{42} oligomers and reduce their deleterious cytotoxic effects on dendritic spines in mouse organotypic hippocampal neural cultures.[19] If initiated at early stages during the clinical management of AD, these and related studies suggest that decreasing the level of soluble Aβ_{42} oligomers while increasing the clearance of these highly toxic species from the brain will help reduce neuronal deterioration in the cortex and hippocampus.

Considering that soluble Aβ_{42} oligomers and chronic inflammation enhance AD pathogenesis, several clinical trials have been initiated to examine anti-inflammatory candidates. The first AD study with NSAIDs failed because trial participants started these treatments when the disease was too advanced.[11,15] Subsequent trials with patients at earlier stages of the disease, including presymptomatic stage patients, are currently ongoing; results from these studies will clarify if anti-inflammatory therapeutics can slow down or even prevent AD in selected patient subpopulations where intervention is started at an early, nonsymptomatic stage. Several nanotechnology-based drug delivery systems and nanoparticles have also been studied for the treatment of AD.[20−22]

Among the nanotechnological products with intrinsic anti-inflammatory activity are dendrimeric polyglycerol sulfates (dPGS, Figure 1A), with or without cleavable ester bonds.[23−27] The architecture of dPGS affects inflammatory processes and hemo-compatibility.[28] The degree of branching and uniformity plays a critical role in the multivalent interactions of dPGS with biological macromolecules.[28] One attraction of dendrimers is their ease of production, reproducibility, and suitability for clinical trials not only because of these technological advantages, but also because they are active at a low nanomolar concentrations and they can be optimized depending on the degree of branching (60%).[28] The distribution and anti-inflammatory properties of highly biocompatible dPGS have been tested in vivo and in vitro.[29−31]

We have previously shown that several anti-inflammatory agents, with or without nanodelivery systems, can normalize the status of hyperactive microglia.[32] Using lipopolysaccharide (LPS) to stimulate microglial activation, dPGS was able to reduce cytokine release from hyperactive microglia and rescue LPS-induced dendritic spine loss at the postsynaptic sites of hippocampal pyramidal neurons.[23] Since the role of reactive astrocytes induced by Aβ_{42} was not addressed in these previous publications, the current study was designed to establish if: (i) dPGS binds to Aβ_{42} and reduces its deleterious effects on spines; (ii) dPGS is internalized by neuroglia and exerts is protective effects indirectly on neurons; (iii) dPGS modulates lipocalin-2 (LCN2) previously suggested as a dendritic spine disruptor. Our new findings suggest that the mechanism of dPGS action involves direct binding to the neurotoxic Aβ_{42} peptide. Moreover, we found a significant upregulation of LCN2 in enriched astrocytes exposed to Aβ_{42} or the proinflammagen LPS. We propose that the astrocytic cytokine LCN2 is a regulator of synaptic circuitries in the central nervous system when exposed to Aβ_{42}, and that dPGS can modulate its deleterious effect mainly through the attenuation of neuroglial activity.

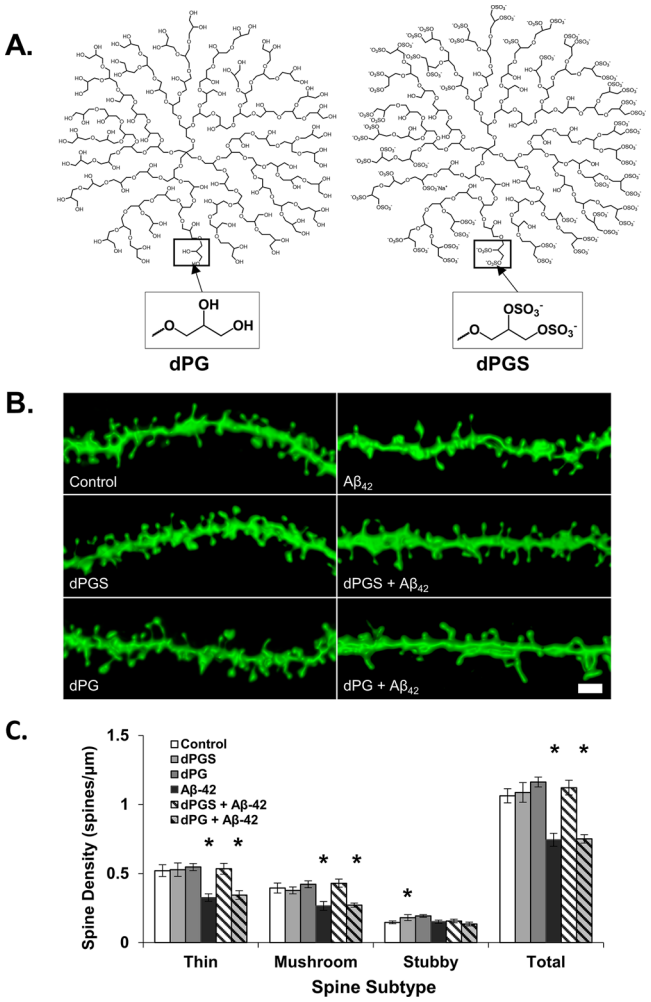

Figure 1. dPGS but not dPG normalizes the morphology of excitatory postsynaptic dendritic spines exposed to Aβ_{42}. (A) Molecular structures of hydroxylated dPG and sulfated dPGS. (B) Representative photomicrographs of dendritic spines exposed to 1 μM Aβ_{42}, dPG, or dPGS alone or in combination for 48 h; 2 μm scale bar is indicated at the bottom right. (C) Quantification of spine density and subtype exposed to above conditions. $n \geq 14$ spine segments from at least four independent samples. Statistical significance was assessed for each spine subtype using ANOVA followed by Dunnett's test. *$p < 0.05$ compared to control.

RESULTS AND DISCUSSION

Synaptic pathology has been linked to many neurological disorders. For example, autopsy specimens have permitted the quantification of synapses in human brain tissue of AD-afflicted individuals. The progression of synaptic loss and testing of candidate therapeutics have been followed in humanized rodents or in vitro in transfected cells.[33−35]

Using complementary techniques, we investigated if dPGS can prevent the deterioration of excitatory hippocampal synapses in the presence of Aβ_{42}, and tested for direct binding between dPGS and Aβ_{42}. Primary mouse cortical cultures as well as organotypic hippocampal cultures were used to test

DOI: 10.1021/acschemneuro.7b00301
ACS Chem. Neurosci. 2018, 9, 260−271

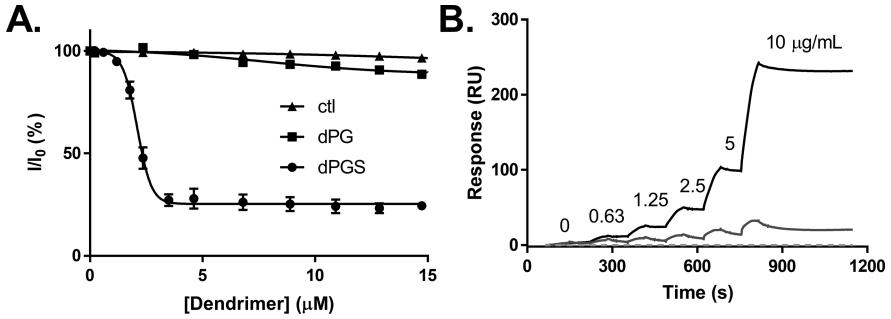

Figure 2. dPGS directly binds to Aβ_{42}. (A) Representative extrinsic fluorescence in which fixed Aβ_{42}-HiLyte647 concentration (200 nM) was titrated against itself (triangles, negative control), dPG (squares, negative control), and dPGS (circles, specific dose-dependent quenching); nonlinear regression analysis (black line) predicts apparent equilibrium dissociation (K_D) constant of ~2 μM). (B) Representative SPR in which buffer (dashed line), Aβ_{40} (gray line), and Aβ_{42} (black line) were titrated over dPGS sensors (specific dose-dependent binding after subtraction over matching dPG reference surfaces).

nanotechnological dendrimeric structures as modulators of glial activation and morphological changes of postsynaptic dendritic spine subtypes.

Organotypic brain tissue cultures represent an attractive approach to screen the effect of therapeutic candidates on dendritic spines that are essential for human synaptic function. In the context of neuroinflammatory processes in AD pathogenesis, the cultures were exposed to neurotoxic Aβ_{42} species in the absence or presence of dPGS to assess the intrinsic anti-inflammatory properties of these dendrimers and their ability to attenuate deleterious effects of hyperactive neuroglia.

dPGS Prevents Aβ-Induced Damage at the Hippocampal Excitatory Synapses. We hypothesized that dPGS (Figure 1A) would rescue the loss of postsynaptic dendritic spines in organotypic hippocampal slices exposed to toxic Aβ_{42} through several mechanisms. We first imaged and quantified excitatory synapses in organotypic cultures from transgenic mice expressing green fluorescent protein (GFP) in a subgroup of population of hippocampal neurons in CA1 region.[36] A significant decrease in total dendritic spine number was observed after 2 days of exposure to Aβ_{42}, with notable sensitivity in the thin as well as larger, stronger "mushroom" spine population (Figure 1B,C).

In organotypic hippocampal cultures, both the morphology and organization of neural circuitries are retained, and direct interactions between astrocytes and dendrites can be revealed.[37] This astrocyte-dendrite interaction is of relevance because neuroglia can modulate circuitry functions both positively and negatively.[38] It was shown that hyperactive microglia and reactive astrocytes can adversely affect synaptic plasticity. Considering that astrocytes and microglia internalize dPGS (see Results and Discussion), we propose that reactive glia were normalized by dPGS treatments, suggesting a switch from a hyperactive (microglia) and reactive state (A1 astrocytes) to the spectrum of more physiologically active states (surveying microglia and A2 astrocytes).[9] Our earlier studies showed that dPGS was avidly taken up by microglia and prevented the loss of spines after LPS exposure.[23] In the present study, we demonstrate that dPGS was able to rescue the loss of thin, mushroom, and total spine density in cultures exposed to Aβ_{42} ($p < 0.05$, ANOVA and post hoc Dunnett's test) (Figure 1B,C). This dPGS-mediated prevention of spine density loss is consistent with our previous studies where an Aβ-oligomer interacting peptide (AIP) was also able to neutralize toxic Aβ_{42} species and protect synaptic structure and function.[19] Interestingly, dPG was neither toxic to spines nor protective against spine loss caused by Aβ_{42}.

dPGS Interacts Directly with Aβ and Impairs Fibril Formation. Since Aβ_{42}-induced spine loss can be prevented by dPGS treatment, this prompted us to question if dPGS directly binds to Aβ_{42}, and, if so, whether it affects its aggregation. We employed a series of orthogonal biophysical techniques to answer these questions.

Fluorescence Spectroscopy (Extrinsic). To first test for direct binding between dPGS and Aβ in solution, the same fluorescently labeled Aβ_{42} used in our cell-based assays was then tested by extrinsic fluorescence measurement. A fixed concentration of Aβ_{42}-HiLyte647 (200 nM) was titrated in the presence of increasing concentration of dPG or dPGS (Figure 2A). Fluorescence intensity of the extrinsic HiLyte647 label decreased in a sigmoidal fashion as a function of dPGS concentration with an inflection point at 10-fold excess of dPGS to Aβ (2.1 μM). Using either the hydroxylated polyglycerol dendrimer lacking the sulfate groups (dPG, with similar M_w) or titrating 200 nM Aβ_{42}-HiLyte647 against itself did not significantly alter the starting fluorescence signals (Figure 2A). While dPGS did not cause any quenching using a 1:5 ratio between Aβ_{42}-HiLyte647 and dPGS, significant signal decreases were detected using molar ratios of 1:10 and higher (i.e., Aβ_{42}-HiLyte647:dPGS). The specific, dose-dependent reduction in fluorescence intensity with increasing dPGS concentrations indicates direct binding between dPGS and Aβ_{42}-HiLyte647.

Surface Plasmon Resonance (SPR). To then test for direct binding between dPGS and Aβ peptides in the absence of fluorescent tags, SPR experiments were performed with both the less-toxic, less-aggregating Aβ_{40} and the more toxic, aggregation-prone Aβ_{42}. There was little or no response when both peptides were titrated over dendritic polyglycerols with exposed hydroxyl groups (i.e., dPG reference surfaces, Supplementary Figure 1A), as compared to the significant, concentration-dependent binding over dendritic polyglycerols with exposed sulfate groups (i.e., active dPGS surfaces) (Supplementary Figure 1B). Across identical titration ranges, the final reference-subtracted data (Figure 2B) showed that (i) the signal responses with freshly dissolved Aβ_{42} (predominantly 4512 Da monomer with additional oligomeric species) were significantly larger compared to freshly dissolved Aβ_{40} (4329 Da monomeric), and (ii) the dPGS-Aβ complex is stable, as evidenced by the slow dissociation rates observed. While the micromolar titration ranges in the SPR (i.e., 10 μg mL^{-1} Aβ =

DOI: 10.1021/acschemneuro.7b00301
ACS Chem. Neurosci. 2018, 9, 260−271

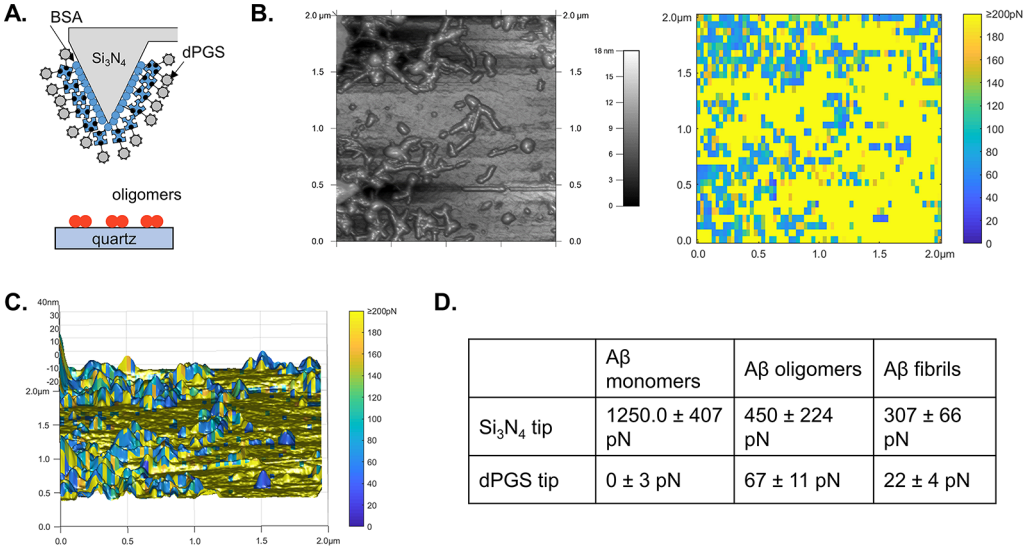

	Aβ monomers	Aβ oligomers	Aβ fibrils
Si_3N_4 tip	1250.0 ± 407 pN	450 ± 224 pN	307 ± 66 pN
dPGS tip	0 ± 3 pN	67 ± 11 pN	22 ± 4 pN

Figure 3. AFM determination of dPGS interaction with Aβ_{42} species. (A) Schematic of dPGS-coated AFM cantilever tips (BSA-biotin/streptavidin/dPGS-biotin) and Aβ peptides deposited on O_3-treated quartz surface. (B) AFM micrograph of Aβ_{42} oligomeric species imaged with dPGS-coated cantilever tips and corresponding adhesion map. (C) Superimposition of the adhesion map (color) on top of topography of Aβ oligomer structures. (D) Table of average adhesion forces measured between bare silica nitride cantilever tips or dPGS-coated tips and Aβ peptide populations (shaken for 0, 8, or 24 h at 37 °C and 450 rpm).

approximately 2 μM, if predominantly 4512 Da monomer) are consistent with our earlier fluorescence titrations (0−20 μM dendrimer), we suspect that avidity effects likely account for the slower than expected SPR dissociation kinetics. Thus, the inherent heterogeneity in dPGS (multivalent) and/or Aβ_{42} (mixture of monomers and low-order oligomers) hindered our ability to determine a reliable equilibrium dissociation constant (K_D) in the SPR experiments.

There is evidence that heparin sulfate (HS) of heparan sulfate proteoglycans (HSPGs), a form of glycosaminoglycan (GAG),[39,40] play a role in amyloid plaque stability. In addition to cell-anchored GAGs, soluble GAGs such as heparin are distributed in the body. Heparin possesses anticoagulant and anti-inflammatory properties that are mediated by the interaction with distinct serum proteins, cell receptors, and other heparin binding site-containing proteins, such as amyloid precursor protein (APP). The heparin sulfate chain on HSPGs binds to a diverse array of ligands, ranging from cytokines, to growth factors and enzymes and can protect them against proteolysis.[41] HSPGs are abundant cell surface molecules, and have been associated with Aβ aggregation and deposition. Amyloid fibrils can themselves behave as polyelectrolytes and interact with such bearing the opposite charge.

The direct interaction between the histidine-rich region of human Aβ (residues 12−18) and the trisaccharide sequence of heparin, a highly sulfated form of HS, is mediated by electrostatic interactions, and the strength of this correlates with the size of the oligosaccharide.[42] The strength and the specificity of individual polyanion-protein interactions are determined by multiple factors (e.g., charge density, character, patterning, and size) and affect pathogen defense mechanisms, tissue integrity, cell migration, protein folding, and neurodegenerative processes.[43]

Blockage of the interaction of the different soluble Aβ peptide species that are prone to aggregation with polyanions is supposed to interfere with amyloid formation, and thus, prevent damage of neuronal tissue. Our results reveal that synthetic dPGS polymer, in contrast to dPG, exhibits a particular propensity to interact with Aβ_{42}, as compared to Aβ_{40}. Freshly dissolved Aβ_{42} peptides contain a larger amount of low-order oligomers that show a higher avidity based on multimeric interactions. This seems to be a general property displayed by aggregated forms of proteins like muscle acylphosphatase and human lysozyme in the interaction with biological polyelectrolytes.[44] Such interpretation is further supported by our EM results, showing that dPGS stabilize low-order aggregated states of Aβ, likely through compensation of electrostatic repulsion as previously observed for heparin and the acylphosphatase.[44]

The ability of dPGS to directly interact with Aβ may enable dPGS to "trap" Aβ oligomers and neutralize their toxic effects by inhibiting toxic fibril formation (i.e., amyloidosis). This may be therapeutically relevant considering the dPGS intrinsic anti-inflammatory properties. Applying anti-inflammatory polyanions to combat Aβ-aggregation in the brain is especially promising because reducing toxic oligomer buildup and local inflammation may solve the root cause of AD.

Atomic Force Microscopy (AFM). To cross-validate the dPGS-Aβ_{42} interaction detected by fluorescence and SPR, we also performed atomic force microscopy (AFM). Biotinylated dPGS was captured to streptavidin-coated, BSA-blocked cantilevers and Aβ_{42} was layered to custom-made quartz surfaces through hydrogen bonding (Figure 3A). The samples were first imaged in amplitude modulation mode in order to spatially locate the Aβ_{42} species and measure their spatial dimensions (left inset of Figure 3B shows a height image of an oligomer sample). A map of the adhesion between dPGS and the surface for the same area was then obtained by performing 2048 force−distance curves (right inset of Figure 3B). From these force−distance curves, the interaction between molecules, or adhesion force, was calculated. The adhesion map superimposed on the topography shows that when dPGS interacts with oligomers, the adhesion force is relatively small compared to dPGS interacting with quartz (Figure 3C). This indicates that the measured force on oligomers is due to their interaction with dPGS, and not that of the underlying surface. The interaction is also not due to the underlying tip material

DOI: 10.1021/acschemneuro.7b00301
ACS Chem. Neurosci. 2018, 9, 260−271

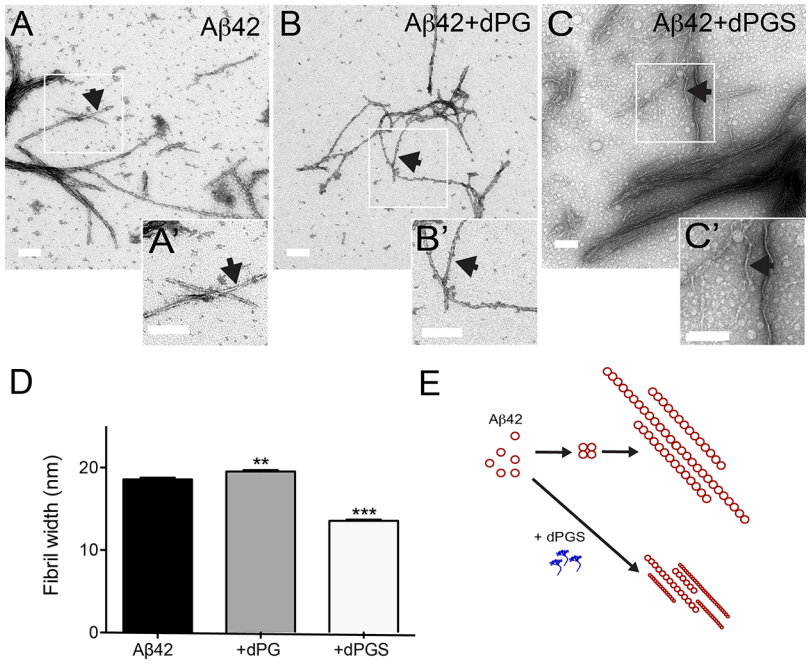

Figure 4. Aβ_{42} fibril formation is impaired by dPGS. Freshly resuspended Aβ_{42} monomers were allowed to aggregate for 24 h at 37 °C, prior to negative staining and visualization by TEM (scale bar = 100 nm). (A) In the absence of dPG or dPGS, the Aβ_{42} aggregates are a homogeneous population of long, mature fibrils with *similar width* (18.57 ± 0.21 nm). (B) In the presence of equimolar dPG, the Aβ_{42} aggregates are a homogeneous population of fibrils with similar length but moderately *increased width* (19.52 ± 0.17 nm). (C) In the presence of equimolar dPGS, the Aβ_{42} aggregates are a heterogeneous population of short and long fibrils with *reduced width* (13.55 ± 0.14 nm). The representative TEM images include white boxes that are further enlarged (corresponding A′, B′, and C′ panels) to highlight the sample fibrils (*black arrows*). (D) average fibril widths were determined by taking three measurements along each fibril using Metamorph software. The following number of fibrils was analyzed for each condition: Aβ_{42} (control) n = 143; Aβ_{42} + dPG n = 284; Aβ_{42} + dPGS n = 457. $^{**}p < 0.01$, $^{***}p < 0.001$, Dunnett's post hoc test). (E) Proposed mechanism: dPGS interacts with Aβ_{42} aggregates during the oligomerization and/or elongation phases to ultimately impair mature fibril formation.

since uncoated Si_3N_4 tips showed a much larger adhesion force with all Aβ species than the dPGS coated tips (see table in Figure 3D).

The interaction between dPGS and Aβ_{42} oligomers (67 ± 11 pN) is significantly larger than the interaction between dPGS and Aβ_{42} fibrils (22 ± 4 pN) and between dPGS and Aβ_{42} monomers (0 ± 3 pN).

Transmission Electron Microscopy (TEM). To complement the AFM studies, we performed TEM analysis to characterize fibril morphologies, particularly their width. Linked to the progression and severity of AD, previous literature has detected structural variations in the Aβ fibrils extracted from the brains of AD patients.[45] Moreover, our previous size-exclusion chromatography (SEC) and TEM studies have shown that the time-dependent formation of toxic Aβ oligomeric species occurs 4−8 h following resuspension, and mature fibrilization by 24 h.[19,46]

For freshly resuspended Aβ_{42} peptides (i.e., predominantly monomeric) that were allowed to aggregate for 24 h at 37 °C (physiologically relevant temperature), our TEM analyses detected the formation of mature, long fibrils with similarly consistent widths (Figure 4A and inset A′). Although equimolar dPG did not appear to alter the length of Aβ_{42} fibrils, their widths did appear to modestly increase in its presence (Figure 4B and inset B′). Interestingly, the presence of equimolar dPGS resulted in greater variability−fewer fibrils overall, including many shorter and thinner ones (Figure 4C and inset C′). Since many fibrils appeared twisted and in clusters, we could only reliably quantify the widths of the fibrils and not the lengths (Figure 4D). Overall, significantly thinner fibrils were formed in the presence of dPGS (13.55 ± 0.14 nm) compared to dPG (19.53 ± 0.17 nm) or Aβ_{42} alone (18.57 ± 0.21 nm). Our TEM data (Figure 4E) suggests that dPGS can interact with low-n Aβ_{42} oligomers (i.e., consistent with direct binding in extrinsic fluorescence, SPR, and AFM assays) and alter the formation of higher-order aggregates (i.e., consistent with shorter, thinner fibrils observed by TEM). Overall, these data are reminiscent of our previous findings where a small molecule NSAID (sulindac sulfide) could alter the self-association of Aβ_{42}, ultimately forming oligomeric aggregates with reduced neurotoxicity.[18] As a novel strategy to prevent toxic amyloid formation, dPGS is a desirable candidate if it can alter the aggregation of Aβ_{42} to prevent the formation of mature fibrils.

dPGS Effects on Neuroglia. *dPGS Is Internalized by Astrocytes and Microglia.* Considering that microglia and astrocytes take up Aβ species, communicate with neurons, and can form multipartite synapses, we focused on neuroglia as modulators of circuitry functions. We investigated whether dPGS is internalized by neuroglia or if its effects are strictly in the extracellular milieu. We treated primary enriched astrocytes and microglia with 0.1 μM and 1 μM dPGS-Cy5 for 2 and 24 h and immunolabeled astrocytes with antibodies against glial fibrillary acidic protein (GFAP) and microglia with antibodies against ionized calcium-binding adapter molecule-1 (Iba-1). While fluorescently labeled dPGS was detectable in both primary astrocytes and microglia, there were striking differences in the amount of dPGS taken up by these cells. Following 2 h of treatment with either 0.1 or 1 μM dPGS-Cy5, there was

DOI: 10.1021/acschemneuro.7b00301
ACS Chem. Neurosci. 2018, 9, 260−271

virtually no dPGS internalized by astrocytes, as evidenced by the absence of intracellular Cy5 fluorescence (Figure 5A). In

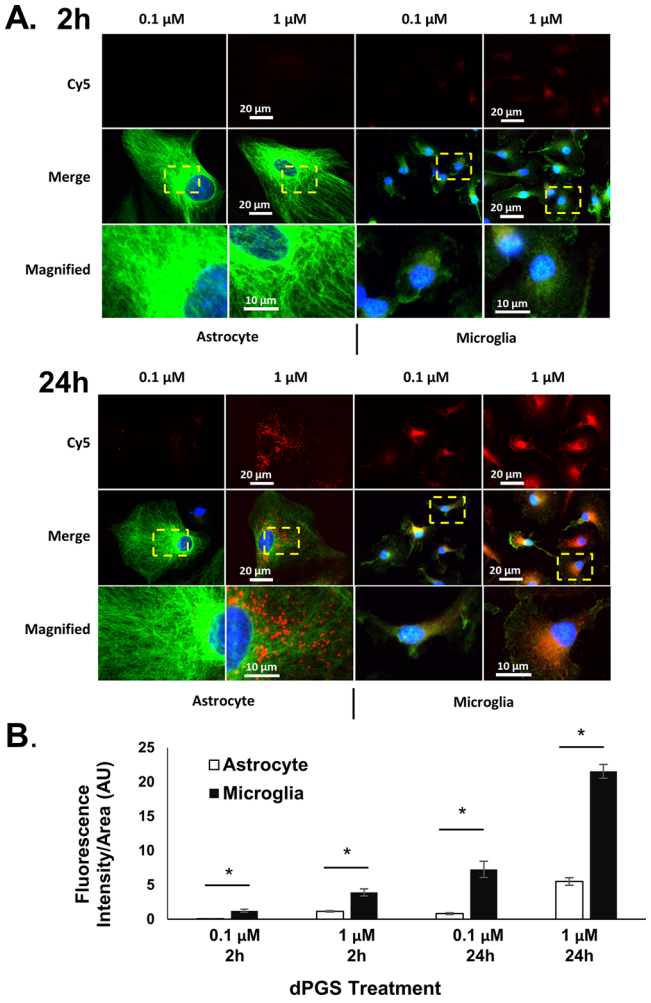

Figure 5. Uptake of dPGS-Cy5 in enriched astrocyte and microglia cultures. (A) Representative photomicrographs of astrocytes and microglia treated with 0.1 and 1 μM dPGS-Cy5 (shown in red) for 2 and 24 h. Astrocytes were immunolabeled for GFAP (shown in green) and microglia with Iba-1 (shown in green). Nuclei were labeled with Hoechst 33342 (shown in blue). (B) Quantification of dPGS-Cy5 fluorescence/cell area in astrocytes and microglia. Quantified from four independent experiments, data represents mean ± SEM.

contrast, the 2 h treatment was sufficient to detect low levels of 0.1 and 1 μM dPGS uptake in microglia, concurring with our previous findings that microglia are the first neural cells to internalize dPGS.[23] Following a similar 24 h treatment, the uptake of 1 μM dPGS was detectable in astrocytes (Figure 5A). Overall, these results (Figure 5B) show (i) that both astrocytes and microglia internalize dPGS, but at different rates, and (ii) that dPGS uptake by astrocytes is only significant with high 1 μM concentration. Similarly, dPGS uptake in organotypic slices can only be detected following the treatment with 1 μM dPGS-Cy5 (Supplementary Figure 2).

Aβ Content in Neuroglia Is Significantly Reduced in the Presence of dPGS. Data from several studies have suggested that the internalization of monomeric and oligomeric Aβ_{42} species engages different uptake mechanisms including pinocytosis (monomers) and may involve scavenger receptors in microglia.[47] As such, we wanted to determine whether dPGS could diminish or enhance the internalization of Aβ species. To answer this question, we incubated primary astrocytes and microglia with dPGS for 1 h and then added 1 μg mL^{-1} Aβ_{42}-HiLyte647 for 2 and 24 h (Figure 6). A fluorescent signal of Aβ_{42}-HiLyte647 was significantly reduced, suggesting that (i) interaction between Aβ_{42} and dPGS reduced its uptake in neuroglia, (ii) dPGS promoted the elimination of Aβ_{42}-HiLyte647, or (iii) it was an artifact due to the quenching. We excluded the latter possibility since there was no significant reduction of Aβ_{42}-HiLyte647 in the presence of 5-fold higher concentration of dPGS. The quenching phenomenon only occurred with high molar ratios (>10-fold). In addition, there was no change in the lifetime of HiLyte647 when Aβ_{42}-HiLyte647 was combined with equimolar concentration of dPGS (Supplementary Figure 3). The finding that the content of fluorescently labeled Aβ_{42} was reduced in neuroglia was intriguing and the possibility that dPGS could have facilitated elimination of Aβ_{42} merits further investigation. It was reported that autophagic flux and lysosomal functions are reduced with aging and that these impairments lead to an accumulation of internalized materials and degradation products including Aβ_{42} species.[48−52]

Proposed Model. Our data suggest that dPGS can prevent the reduction of spines exposed to Aβ_{42} through direct interaction with Aβ_{42} (mainly oligomeric species), and through modulation of neuroglia. dPGS association with Aβ_{42} involves weak, but multivalent interactions as assessed by complementary biophysical techniques. Both the astrocytes and microglia take up Aβ_{42} and dPGS. dPGS reduces the content of Aβ_{42} in neuroglia and modulates lipocalin-2 (LCN2) secretion from reactive astrocytes.

Considering that reactive astrocytes produce proinflammatory cytokines and lipocalins, we studied if LCN2 is produced by astrocytes exposed to Aβ_{42}, and if dPGS could modulate its synthesis and release. LCN2 is a secreted cytokine exhibiting diverse cellular functions and it is an emerging modulator of dendritic spine morphology and maturation.[53−56] It is induced and upregulated by different stressful stimuli, e.g., inflammation, stroke, and Aβ.[53] Under physiological conditions and in neural cultures not exposed to stimuli, LCN2 is not detectable. In contrast, LCN2 is highly upregulated during trauma and CNS infections.[57] LCN2 release is linked to glial activation and neuronal degeneration.[58,59] Recent studies by Dekens and coworkers, suggest a brain region-specific upregulation of LCN2 in AD.[60] Individuals with AD show a significant increase of LCN2 in the hippocampus and an even more dramatic increase in the brain structure of depressed AD patients.

We measured intracellular and secreted LCN2 in primary mouse cortical neural cultures. Aβ_{42} upregulated LCN2 in primary astrocytes, in dissociated cultures as well as in organotypic cultures (Supplementary Figures 4A and 5). Interestingly, coincubation of equimolar Aβ_{42} and dPGS significantly reduced the percentage of astrocytes positively labeled for LCN2 and LCN2 released into the media (Figure 7). Similarly, in hippocampal slice cultures, equimolar dPGS and Aβ_{42} coincubation reduces LCN2 produced compared to Aβ_{42} incubation alone (Supplementary Figure 4B). Earlier observations suggest astrocyte secrete cytokines which are crucial for the neurotoxic effects of Aβ_{42}.[61] We tested whether recombinant mouse LCN2 (rLCN2) incubation would alter spine morphology in hippocampal slice cultures. Treatment with 100 ng mL^{-1} rLCN2 significantly reduced the total spine density and the thin, mushroom subtypes (Supplementary

DOI: 10.1021/acschemneuro.7b00301
ACS Chem. Neurosci. 2018, 9, 260−271

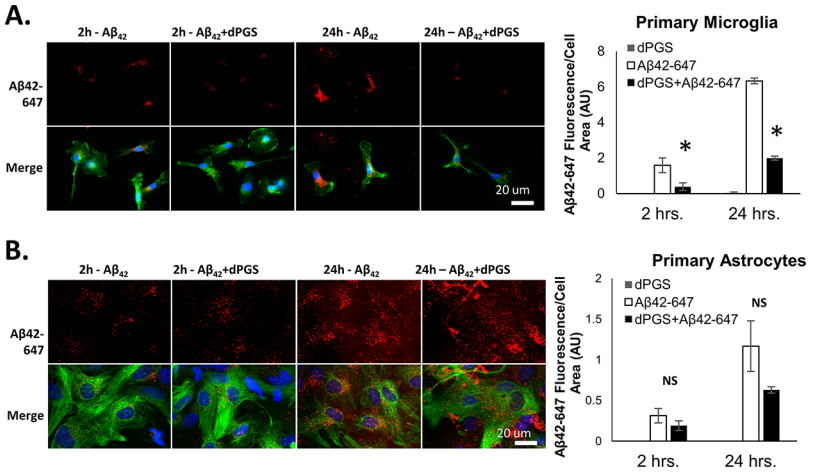

Figure 6. dPGS decrease Aβ_{42}-HiLyte647 uptake in microglia. (A,B) Photomicrographs from primary microglia (A) and primary astrocytes (B) pretreated for 1 h with 1 μM dPGS and treated with 180 nM Aβ_{42}-HiLyte647 (shown in red) for 2 or 24 h. Microglia were immunolabeled with Iba-1 (A) in green, astrocytes with GFAP (B). Nuclei were labeled with Hoechst 33342 (shown in blue). Bar graphs shows Aβ_{42}-647 fluorescence/cell area measurements in the absence and presence of dPGS in microglia (n = 3), astrocyte (n = 4), data represents mean ± SEM, *p < 0.05.

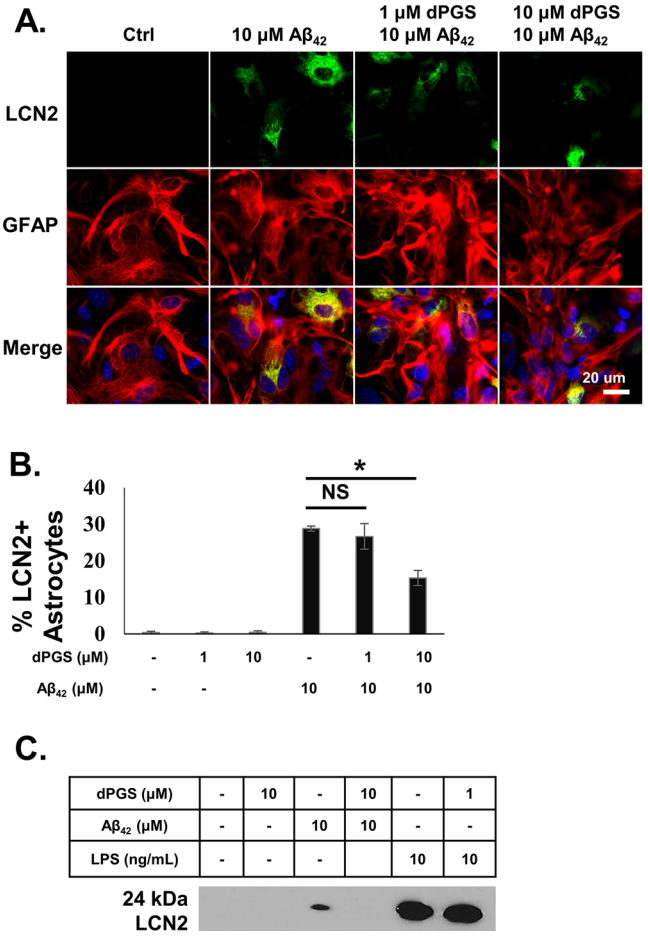

Figure 7. dPGS downregulates Aβ_{42} induced LCN2. (A) Photomicrographs of primary astrocytes pretreated with 1 and 10 μM dPGS for 3 h before adding 10 μM Aβ_{42} for 48 h. Equimolar concentrations of dPGS to Aβ_{42} decreased LCN2 production in astrocytes. Green, LCN2; red, GFAP; blue, nucleus. (B) Count of the percentage of LCN2+ cells of total GFAP+ cells (astrocytes) from three independent experiments, data represent mean ± SEM, *p < 0.05. (C) Medium from treated cells blotted for LCN2. Cells were treated with LPS for 24 h at 10 ng mL^{-1}.

Figure 4C). Similarly, anti-LCN-2 antibody treatment partly rescued spine loss due to Aβ_{42} (Supplementary Figure 4D). Previously published experiments and our own data support the disruptive role of LCN2 on dendritic spines.[56]

Therapeutic interventions which normalizes of LCN2 levels and other disease biomarkers could be a viable strategy to attenuate the severity of neurological disorders such as AD. This study provides the first example of LCN2 regulation with an anti-inflammatory dendritic macromolecule (Figure 8B) and suggests that other (nano)therapeutic strategies warrant further investigation in animal models and eventually in humans with neurological disorders. Recently, exciting imaging data using positron emission tomography (PET) tracers showed that visualization of synaptic density is achievable noninvasively in humans.[62] This study creates new possibilities to evaluate the progression of AD from presymptomatic early stages to full-blown disease in humans, as well as the assessment of therapeutic interventions at the synaptic level.

LCN2 alone and with other released proinflammatory cytokines from reactive astrocytes upon Aβ_{42} exposure, reduces hippocampal spines density which can be prevented by dPGS treatment. Considering anti-inflammatory properties and biocompatibility of dPGS in vivo, testing of dPGS in animal models of AD and for other neurodegenerative disorders is warranted.

METHODS

dPGS Synthesis. dPGS was synthesized according to Türk et al.[63] In brief, dendritic polyglycerol was dissolved in anhydrous DMF and heated to 60 °C. Then SO_3·pyridine complex (1.3 equiv per OH group) in dry DMF was added dropwise and the mixture was stirred overnight at 60 °C. After cooling, water was added and the pH was adjusted to 7 by adding aq. NaOH (10%). The solvent was removed, and the crude product subjected to ultrafiltration in a sodium chloride solution for three cycles and water for five cycles. The compound was obtained as colorless solid after freeze-drying and characterized by ^{1}H NMR, and the sulfate content was determined by elemental analysis.

Synthetic Aβ Peptides. Unlabeled or HiLyte647-labeled human Aβ peptides were purchased from Bachem or Anaspec, respectively. They were monomerized in formic acid and lyophilized into aliquots (average ratio monomers/dimers/oligomers = 55:30:15).[64] To enrich for monomers just prior to experiments, aliquots were freshly resuspended and sonicated in 0.13% ammonium hydroxide solution

DOI: 10.1021/acschemneuro.7b00301
ACS Chem. Neurosci. 2018, 9, 260−271

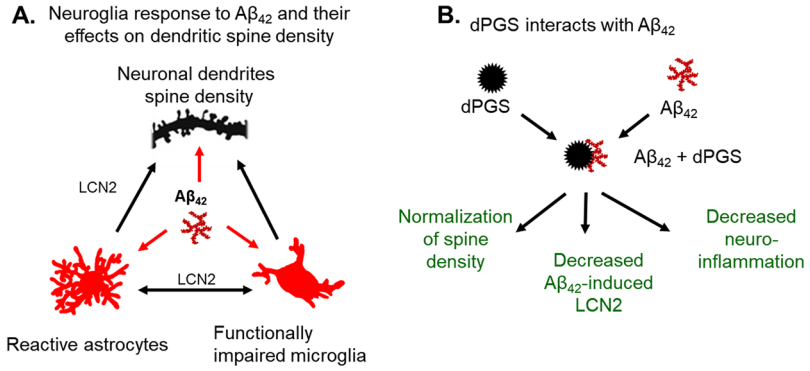

Figure 8. (A) Relationship between neuroglia and upregulation of LCN2 with Aβ_{42} treatment. (B) Interaction between dPGS dendrimer and Aβ oligomeric species and anticipated outcomes.

(1 mg mL^{-1} peptide, final concentration).[65] Based upon our previous size-exclusion chromatography (SEC) and transmission electron microscopy (TEM) analyses, we have shown that the time-dependent formation of toxic Aβ oligomeric species occurs 4−8 h following resuspension, and mature fibrilization by 24 h.[19,46] For quality control, each batch of Aβ peptides was pretested on an UltrafleXtreme MALDI-TOF/TOF system (Bruker Daltonics, Bremen, Germany) according to the manufacturer's recommendations (intact mass analysis in reflector-positive mode, as well as Top-Down Sequencing (in-source decay) to verify the N-/C-terminal amino acid sequences).

Mouse Organotypic Hippocampal Slice Cultures and Spine Quantification. Organotypic hippocampal slice cultures were prepared as previously described by Gähwiler et al.[66] Briefly, the slice cultures were prepared from P6−8 transgenic mice that expressed membrane-targeted eGFP under the Thy-1 promoter in a subpopulation of CA1 cells.[67] Following decapitation, hippocampi were dissected, and 400 μm thick transverse slices were made and adhered onto glass coverslips with chicken plasma clot (Cocalico Biologicals; Reamstown, PA). Cultures were maintained in a roller drum incubator at 37 °C for 3 weeks prior to experimentation. Culture medium consisted of 25% heat-inactivated horse serum (Invitrogen GIBCO), 25% Hank's balanced salt solution (Invitrogen GIBCO), and 50% Basal medium Eagle (Invitrogen GIBCO) and was replaced weekly. Following culture preparation, synaptic connections were allowed to re-establish for 3 weeks in vitro. After the initial 3 week period, dendritic spine densities reach a steady state for up to 6 weeks thereafter. Once the slice cultures are ready, they were incubated overnight in serum-free medium and then treatments were applied. At the treatment end point, cultures were fixed in 4% PFA overnight at 4 °C, washed extensively in PBS, and mounted onto microscope slides. eGFP-expressing CA1 pyramidal neurons were imaged. The images were acquired using an upright Leica TCS SP2 confocal microscope (Leica Microsystems, Heidelberg, Germany) equipped with a HCX PL APO 63× NA 1.4 oil immersion objective. Image stacks were collected at Z = 0.25 μm and averaged three times. Image stacks were deconvolved with Huygens Essentials software (Scientific Volume Imaging, Hilversum, The Netherlands) using a full maximum likelihood extrapolation algorithm. Three-dimensional rendering, volume analysis, and dendritic spine quantification was carried out using Imaris (Bitplane, Zurich, Switzerland). For dendritic spine analysis, spines were classified into three main morphological subtypes: stubby, mushroom, and thin-type spines using previously established methods based on the measurements of spine head and neck diameters.[32]

Fluorescence Spectroscopy. Extrinsic fluorescence experiments were performed at 25 °C using a Cary spectrofluorometer (2 mL cuvette with magnetic stir bar; excitation λ = 610 nm; excitation slit width 5 nm; emission slit width 10 nm; emission λ = 637−800 nm; photomultiplier tube (PMT) voltage = 600 V). Freshly resuspended Aβ_{42}-HiLyte647 (M_w = 5449.4 g mol^{-1}; 1 mg mL^{-1} in 0.13% ammonium hydroxide solution) was diluted to 200 nM in Milli-Q water or HEPES (100 μM, pH 7.4, 0.02% (v/v) Tween-20) and placed in the cuvette (1 mL starting volume). Concentrated dPG and dPGS stocks (120 μM each in water or HEPES buffer, also containing 200 nM Aβ_{42}-HiLyte647 to avoid dilution effects) were added to the cuvette in ≤20 μL increments (1.2 mL final cuvette volume). Relative to the starting fluorescence measurement in each titration series, the transformed intensities (I/I_0) were plotted as a function of dendrimer concentration and then subjected to nonlinear regression analysis (one-site binding model in GraphPad).

Surface Plasmon Resonance (SPR). Opposite to the fluorescence assay, the binding between a fixed dendrimer concentration (5−20 kDa dPG or dPGS) and increasing Aβ concentration (0−10 μg mL^{-1}) was examined using label-free, real-time SPR. The experiments were performed using a BIACORE T200 system (GE Healthcare Bio-Sciences AB, Upsala, Sweden; Control software v2.0 and Evaluation software v1.0) at 25 °C using filtered (0.2 μm) and degassed PBS-T buffer (10 mM phosphate, pH 7.4; 150 mM NaCl; 0.05% (v/v) Tween-20).

Bare gold sensors (Biacore SIA Kit Au) were docked in the instrument and the diluted dendrimers (with exposed thioctic acid (TA) tags) were captured directly to adjacent flow cells (reference surfaces = 500 RU dPG-TA; active surfaces = 500 RU dPGS-TA). In single-cycle kinetics mode, freshly resuspended Aβ peptides (0−10 μg mL^{-1}; 2-fold dilution series) were titrated over the dPG (negative) and dPGS (positive) surfaces at 25 μL min^{-1} (60 s association +30−300 s dissociation). Between titration series, the surfaces were regenerated at 50 μL min^{-1} using two 30 s pulses of PBS-T buffer containing 1.0 M NaCl and 0.05% (v/v) Empigen detergent (Anatrace). All double-referenced data presented are representative of duplicate injections acquired from at least three independent trials.[68]

Atomic Force Microscopy. Relative binding strengths of the peptide were evaluated using MFP-3D atomic force microscope from Asylum Research, Santa Barbara, CA. Force measurements were taken at constant loading rates (vertical piezo velocity of 1 μm s^{-1}). The spring constant of the cantilevers were calibrated in the presence of PBS solution by the thermal fluctuation method. The spring constants were found to be between 0.1−0.5 N m^{-1}. The cantilever tips were coated with biotinylated polyglycerol sulfate (dPGS) dendrimers using the following method: The AFM cantilever tips were incubated in 1 μg mL^{-1} biotinylated bovine serum albumin (BBSA; Sigma) solution in PBS-T (PBS with 0.02% Tween-20), pH 7.0, at room temperature overnight. The tip was incubated for 30 min in 100 μg mL^{-1} streptavidin in PBS-T, and in BSA (1%) for 1 h to block the nonspecific binding sites. Finally, the tip was incubated in dPGS-biotin (1 μM) for 1 h. All these steps were separated by thorough rinsing. Biotinylated dPGS was fixed on the tip prior to each measurement.

The sample, monomerized Aβ_{42} peptide, was freshly resuspended (1 mg mL^{-1} in 0.13% ammonium hydroxide solution) and diluted five times in PBS (10 mM, pH 7.4, NaCl 150 mM). The sample (10 μL) was deposited on a clean quartz slide decontaminated by a 20 min treatment in UVO-Cleaner 42 (Jelight company Inc., Irvine, CA). AFM images were taken for Aβ_{42} which was deposited either immediately after dilution (majority are monomers), after 8 h of

DOI: 10.1021/acschemneuro.7b00301
ACS Chem. Neurosci. 2018, 9, 260−271

agitation at 450 rpm and 37 °C (majority are oligomers), or after 24 h of agitation at 450 rpm and 37 °C (majority of fibrils).

Transmission Electron Microscopy (TEM) Analysis. Freshly dissolved monomerized Aβ_{42} peptides were diluted in PBS pH 7.4 and allowed to aggregate for 24 h at 37 °C in the presence and absence of dPG or dPGS. Aliquots were taken and spotted onto Formvar film-coated nickel electron microscopy grids for 1 min, excess was blotted off and negatively stained for 1 min with uranyl acetate, as previously described.[19] Samples were visualized via a Philips CM120 transmission electron microscope. The average width of each fiber was determined from three measurements taken at different locations along each fibril using the line tool in Metamorph Microscopy Automation and Image Analysis Software (Molecular Devices).

Primary Cultures. P0-P3 C57BL/6 pups were sacrificed and the cortex or hippocampus placed in ice-cold HBSS. The brain tissue was transferred to culturing media (Dulbecco's modified Eagle's medium (DMEM) + 10% FBS + 1% penicillin-streptomycin), dissociated to the single cell level by trituration with a fire-polished pipet, and plated onto poly D-lysine coated T-75 culturing dishes. After 7−8 days in culture, the mixed neural cells (neurons and glia) in culture were shaken in a 37 °C shaker-incubator (G24 Environmental Incubator Shaker, New Brunswick Scientific) for 2 h at 200 rpm to isolate the microglia which were subsequently plated. Cells in the T-75 flask was further shaken for 6−8 h at 260 rpm to remove the oligodendrocyte progenitor cells, and trypsinized to isolate enriched astrocytes. Both microglia and astrocytes were plated onto poly-D-lysine-coated coverslips or seeded into 10 cm^2 dishes and settle for at least 24 h before use. All experiments were conducted in culturing medium unless indicated otherwise. All animal use followed McGill animal use guidelines and were approved by the McGill Facility Animal Care Committees.

Uptake Assays. Primary astrocytes or microglia were treated with 0 (PBS vehicle), 0.1, or 1 μM dPGS-Cy5 for 2 and 24 h. Astrocytes and microglia were fixed and immunostained for GFAP or Iba-1, respectively, using the following immunocytochemistry protocol. Briefly, cells were washed in PBS, then fixed with 4% PFA for 10 min at room temperature, permeabilized with 0.1% Triton-x100 for 10 min at room temperature, blocked for 1 h at RT with 10% goat serum, and incubated with primary antibody overnight at 4 °C (rabbit anti-GFAP (Abcam, 1:1000), rabbit anti-Iba1 (Dako, 1:500). After the primary antibody incubation, cells were incubated with AlexaFluor 488 goat antirabbit (ThermoFisher, 1:500) for 1 h at RT. Nuclei were stained with 10 μM Hoechst 33342 for 10 min at room temperature. Cell were mounted onto microscope slides using Aqua-Poly/Mount (Polysciences, Inc.) and then imaged (Leica inverted fluorescence microscope and/or Zeiss LCM confocal microscope). Using ImageJ software, dPGS-Cy5 uptake was quantified as the total fluorescence per cell normalized per cell area.

Hippocampal organotypic slice cultures were treated with PBS or 1 μM dPGS-Cy5 for 24 h. Slices were fixed with 4% PFA overnight at 4 °C and blocked and permeabilized in blocking buffer (phosphate buffer (PB) + 1.5% horse serum (ThermoFisher) + 0.4% Triton-x100 (Sigma)) overnight at 4 °C. Slices were incubated in rabbit anti-GFAP (Abcam, 1:200) diluted in blocking buffer at 4 °C for 5 days with gentle shaking. Slices were next labeled with goat antirabbit AlexaFluor-488 (ThermoFisher, 1:250) for 3 h at RT with gentle shaking. Samples were mounted onto coverslips using Aqua-polymount (Polysciences, Inc.) and imaged using fluorescence microscopy.

In additional experiments, primary astrocytes or microglia were treated with Aβ_{42}-HiLyte647 (1 μg mL^{-1} for 2 or 24 h) in the absence or presence of dPGS pretreatment (1 μM for 1 h). The cells were fixed, immunostained, and quantified in the similar manner as noted above.

LCN2 Assays. For LCN2 immunocytochemistry, cells were fixed with 4% PFA for 20 min, blocked with PBS + 0.3% Triton-x100 + 0.5% BSA for 1 h at room temperature, and incubated in goat anti-LCN2 (R&D, 1:40) plus rabbit anti-GFAP (Abcam, 1:1000) diluted in blocking buffer for 1 h at RT. Cells were labeled with AlexaFluor-488 donkey antigoat (ThermoFisher, 1:500 diluted in PBS) for 1 h at RT followed by three washes with PBS, and incubated with AlexaFluor-647 goat anti-rabbit (ThermoFischer, 1:500) diluted in PBS for 1 h at RT. Nuclei were stained with 10 μM Hoechst 33342 for 10 min at RT. Cell were mounted onto microscope slides using Aqua-Poly/Mount (Polysciences, Inc.).

For LCN2 immunohistochemistry, hippocampal organotypic slice cultures were treated with PBS or 1 μM Aβ_{42} for 48 h. Slices were fixed with 4% PFA overnight at 4 °C and block and permeabilized in blocking buffer (phosphate buffer (PB) + 1.5% horse serum (ThermoFisher) + 0.4% Triton-x100 (Sigma)) overnight at 4 °C. Slices were incubated in goat anti-LCN2 (R&D, 1:100), rabbit anti-GFAP (Abcam, 1:200), or rabbit anti-Iba1 (1:200, Wako) diluted in blocking buffer at 4 °C for 5 days with gentle shaking. Slices were labeled with donkey anti-goat AlexaFluor-488 or donkey anti-goat AlexaFluor-647 (ThermoFisher, 1:250) for 3 h at RT with gentle shaking. If a cell marker stain was also used (GFAP/Iba-1) samples were extensively washed in PB + 1.5% horse serum and were next labeled with AlexaFluor 647 goat anti-rabbit (ThermoFisher, 1:250) for 3 h at RT with gentle shaking. Samples were mounted onto coverslips using Aqua-polymount (Polysciences, Inc.) and imaged using fluorescence microscopy.

For LCN2 Western blot, primary astrocytes were seeded into 6-well plates and grown to confluence. Cells were lysed in cold RIPA buffer with protease inhibitor cocktail (1 mM sodium orthovanadate, 1 mM phenylmethylsulfonyl fluoride, 1 μg mL^{-1} aprotinin, 1 μg mL^{-1} leupeptin) and briefly sonicated. Protein concentration was determined by BCA assay (Piece BCA Protein Assay Kit, ThermoFisher). The cell culture medium was collected from the tissue culture well and stored at −20 °C. Both cell lysate and cell media samples were mixed in Laemmli sample buffer and heated to 95 °C for 5 min. Samples ran in 10% gradient sodium dodecyl sulfate-polyacrylamide gel electrophoresis (SDS-PAGE) gel for 90 min and transferred onto PVDF membranes. Membranes were blocked with 10% milk TBS-T for 1 h at RT and were incubated with primary antibodies (goat anti-LCN2 (R&D, 1:500), rabbit anti-alpha-tubulin (Abcam, 1:5000)) overnight at 4 °C. Membranes were washed with TBS-T and blotted with secondary antibodies (anti-goat HRP-conjugate (BioRad, 1:1000), anti-rabbit HRP-conjugate (BioRad, 1:1000)) for 1 h at RT. The blot was developed with Clarity Western ECL Substrate and developed exposed to film (HyBlot CL film, Harvard Apparatus). Image processing was performed using ImageJ.

Fluorescence Lifetime Measurements. For Supplementary Figure 3, batch-mode fluorescence lifetimes of the Aβ_{42}-HiLyte were measured by time-correlated single-photon counting (TCSPC) on a Mini-Tau (Edinburgh Instruments, Kirkton campus, UK) and data was analyzed with the F980 software. The excitation source was a 405 nm emitting laser with a frequency set to 20 MHz. The emission for the HiLyte647 dye was detected using filter 6 of the instrument. The emitted photons were counted at 90° from the incident light. The instrument response was determined using filter 1 and toluene in the quartz cuvette. Measurements were stopped after the number of emitted photons counted reached 10 000 photons.

Statistical Analysis. All data are shown as means ± SEM. One-way ANOVAs were combined with Dunnett's post hoc analysis, using the control sample as reference. Alternatively, if appropriate, Student's t test was used to identify significant differences. The changes were considered significant when $p < 0.05$.

■ ASSOCIATED CONTENT

Supporting Information

The Supporting Information is available free of charge on the ACS Publications website at DOI: 10.1021/acschemneuro.7b00301.

Label-free, real-time binding between dPGS and Aβ42; dPGS-Cy5 uptake in astrocytes in organotypic cultures; fluorescence lifetime of Aβ42-HyLite647 in the presence of dPGS; upregulation of LCN2 in response to increasing concentrations of Aβ42 in astrocytes; down-

DOI: 10.1021/acschemneuro.7b00301
ACS Chem. Neurosci. 2018, 9, 260−271

regulation of LCN2 by dPGS in Aβ42-treated organotypic slices; reduction of hippocampal spine density by recombinant-LCN2; antibody neutralization of LCN2 partially rescues spine loss; labeling of LCN2 in astrocytes and microglia in organotypic slices treated with Aβ42 (PDF)

AUTHOR INFORMATION

Corresponding Author

*E-mail: dusica.maysinger@mcgill.ca. Phone +1-514-398-1264. Fax +1-514-398-2045.

ORCID

Dusica Maysinger: 0000-0002-0017-5201

Rainer Haag: 0000-0003-3840-162X

Author Contributions

D.M. and J.J. contributed equally to this work. Senior scientists (D.M., P.G., J.B., R.A.M., R.H., and G.M.) supervised all experiments, participated in discussions, writing, and data analysis. Experiments were performed by graduate students (J.J., I.Z., P.K.Y.C., M.R., M.A., S.R.), postdoctoral fellows (A.M.), and research associates (S.H., M.A.H.). D.M. drafted the manuscript and all authors contributed to the final text. All authors approved the content of the manuscript before submission.

Funding

D.M., R.A.M., J.B., and G.M. acknowledge financial support by the Canadian Institute of Health Research (CIHR; MOP-119425, and MOP-133411). D.M., R.A.M., P.G., and G.M. also acknowledge the support by grants from the Natural Sciences and Engineering Research Council of Canada (NSERC; #RGPIN 04994-15 and Discovery Grant #RGPIN 04774-15). G.M. holds a Canada Research Chair in Molecular Pharmacology. J.B.'s work is supported by McGill University and the Canada Research Chair program. R.A. acknowledges the support by SFB 765 grant. A.M. acknowledges the financial support by Canadian Institutes for Health Research and the SToP-AD Centre, and S.H. by the Alzheimer Society of Canada. The McGill SPR-MS Facility (Department of Pharmacology & Therapeutics) thanks the Canada Foundation for Innovation (CFI) for infrastructure support (Grants #32616, #228340).

Notes

The authors declare no competing financial interest.

ACKNOWLEDGMENTS

Thanks to the McGill EM Facility (Department of Pharmacology & Therapeutics) and Advanced Bioimaging Facility (ABIF; Department of Physiology), respectively, for assistance with the Philips CM120 transmission electron microscope and Metamorph Microscopy Automation and Image Analysis Software.

REFERENCES

(1) Akiyama, H., Barger, S., Barnum, S., Bradt, B., Bauer, J., Cole, G. M., Cooper, N. R., Eikelenboom, P., Emmerling, M., Fiebich, B. L., Finch, C. E., Frautschy, S., Griffin, W. S., Hampel, H., Hull, M., Landreth, G., Lue, L., Mrak, R., Mackenzie, I. R., McGeer, P. L., O'Banion, M. K., Pachter, J., Pasinetti, G., Plata-Salaman, C., Rogers, J., Rydel, R., Shen, Y., Streit, W., Strohmeyer, R., Tooyoma, I., Van Muiswinkel, F. L., Veerhuis, R., Walker, D., Webster, S., Wegrzyniak, B., Wenk, G., and Wyss-Coray, T. (2000) Inflammation and Alzheimer's disease. *Neurobiol. Aging 21*, 383−421.

(2) Cribbs, D. H., Berchtold, N. C., Perreau, V., Coleman, P. D., Rogers, J., Tenner, A. J., and Cotman, C. W. (2012) Extensive innate immune gene activation accompanies brain aging, increasing vulnerability to cognitive decline and neurodegeneration: a microarray study. *J. Neuroinflammation 9*, 179.

(3) Haass, C., and Selkoe, D. J. (2007) Soluble protein oligomers in neurodegeneration: Lessons from the Alzheimer's amyloid beta-peptide. *Nat. Rev. Mol. Cell Biol. 8*, 101−112.

(4) Guillot-Sestier, M. V., and Town, T. (2013) Innate immunity in Alzheimer's disease: A complex affair. *CNS Neurol. Disord.: Drug Targets 12*, 593−607.

(5) Farina, C., Aloisi, F., and Meinl, E. (2007) Astrocytes are active players in cerebral innate immunity. *Trends Immunol. 28*, 138−145.

(6) Chakrabarty, P., Jansen-West, K., Beccard, A., Ceballos-Diaz, C., Levites, Y., Verbeeck, C., Zubair, A. C., Dickson, D., Golde, T. E., and Das, P. (2010) Massive gliosis induced by interleukin-6 suppresses Abeta deposition in vivo: evidence against inflammation as a driving force for amyloid deposition. *FASEB J. 24*, 548−559.

(7) De Kimpe, L., van Haastert, E. S., Kaminari, A., Zwart, R., Rutjes, H., Hoozemans, J. J. M., and Scheper, W. (2013) Intracellular accumulation of aggregated pyroglutamate amyloid beta: convergence of aging and A beta pathology at the lysosome. *Age (Dordrecht, Neth.) 35*, 673−687.

(8) Parihar, M. S., and Brewer, G. J. (2010) Amyloid-beta as a modulator of synaptic plasticity. *J. Alzheimer's Dis. 22*, 741−763.

(9) Liddelow, S. A., Guttenplan, K. A., Clarke, L. E., Bennett, F. C., Bohlen, C. J., Schirmer, L., Bennett, M. L., Munch, A. E., Chung, W. S., Peterson, T. C., Wilton, D. K., Frouin, A., Napier, B. A., Panicker, N., Kumar, M., Buckwalter, M. S., Rowitch, D. H., Dawson, V. L., Dawson, T. M., Stevens, B., and Barres, B. A. (2017) Neurotoxic reactive astrocytes are induced by activated microglia. *Nature 541*, 481−487.

(10) Keren-Shaul, H., Spinrad, A., Weiner, A., Matcovitch-Natan, O., Dvir-Szternfeld, R., Ulland, T. K., David, E., Baruch, K., Lara-Astaiso, D., Toth, B., Itzkovitz, S., Colonna, M., Schwartz, M., and Amit, I. (2017) A unique microglia type associated with restricting development of Alzheimer's disease. *Cell 169*, 1276−1290.

(11) Zandi, P. P., and Breitner, J. C. (2001) Do NSAIDs prevent Alzheimer's disease? And, if so, why? The epidemiological evidence. *Neurobiol. Aging 22*, 811−817.

(12) Breitner, J. C., Baker, L. D., Montine, T. J., Meinert, C. L., Lyketsos, C. G., Ashe, K. H., Brandt, J., Craft, S., Evans, D. E., Green, R. C., Ismail, M. S., Martin, B. K., Mullan, M. J., Sabbagh, M., and Tariot, P. N. (2011) Extended results of the Alzheimer's disease anti-inflammatory prevention trial. *Alzheimer's Dementia 7*, 402−411.

(13) Leoutsakos, J. M., Muthen, B. O., Breitner, J. C., and Lyketsos, C. G. (2012) Effects of non-steroidal anti-inflammatory drug treatments on cognitive decline vary by phase of pre-clinical Alzheimer disease: Findings from the randomized controlled Alzheimer's Disease Anti-inflammatory Prevention Trial. *Inter. J. Geriatr. Psychiatry 27*, 364−374.

(14) Meinert, C. L., McCaffrey, L. D., and Breitner, J. C. (2009) Alzheimer's Disease Anti-inflammatory Prevention Trial: Design, methods, and baseline results. *Alzheimer's Dementia 5*, 93−104.

(15) Breitner, J., Evans, D., Lyketsos, C., Martin, B., and Meinert, C. (2007) ADAPT trial data. *Am. J. Med. 120*, e3−e7.

(16) Breitner, J. C., Martin, B. K., and Meinert, C. L. (2006) The suspension of treatments in ADAPT: Concerns beyond the cardiovascular safety of celecoxib or naproxen. *PLoS Clin. Trials 1*, e41.

(17) Sonnen, J. A., Larson, E. B., Walker, R. L., Haneuse, S., Crane, P. K., Gray, S. L., Breitner, J. C., and Montine, T. J. (2010) Nonsteroidal anti-inflammatory drugs are associated with increased neuritic plaques. *Neurology 75*, 1203−1210.

(18) Prade, E., Barucker, C., Sarkar, R., Althoff-Ospelt, G., Lopez del Amo, J. M., Hossain, S., Zhong, Y., Multhaup, G., and Reif, B. (2016) Sulindac sulfide induces the formation of large oligomeric aggregates of the Alzheimer's disease amyloid-beta peptide which exhibit reduced neurotoxicity. *Biochemistry 55*, 1839−1849.

(19) Barucker, C., Bittner, H. J., Chang, P. K., Cameron, S., Hancock, M. A., Liebsch, F., Hossain, S., Harmeier, A., Shaw, H., Charron, F. M.,

DOI: 10.1021/acschemneuro.7b00301
ACS Chem. Neurosci. 2018, 9, 260−271

Gensler, M., Dembny, P., Zhuang, W., Schmitz, D., Rabe, J. P., Rao, Y., Lurz, R., Hildebrand, P. W., McKinney, R. A., and Multhaup, G. (2015) Abeta42-oligomer Interacting Peptide (AIP) neutralizes toxic amyloid-beta42 species and protects synaptic structure and function. *Sci. Rep. 5*, 15410.
(20) Gao, G. B., Zhang, M. X., Gong, D. J., Chen, R., Hu, X. J., and Sun, T. L. (2017) The size-effect of gold nanoparticles and nanoclusters in the inhibition of amyloid-beta fibrillation. *Nanoscale 9*, 4107−4113.
(21) Savchenko, A., Braun, G. B., and Molokanova, E. (2016) Nanostructured antagonist of extrasynaptic nmda receptors. *Nano Lett. 16*, 5495−5502.
(22) Wen, M. M., El-Salamouni, N. S., El-Refaie, W. M., Hazzah, H. A., Ali, M. M., Tosi, G., Farid, R. M., Blanco-Prieto, M. J., Billa, N., and Hanafy, A. S. (2017) Nanotechnology-based drug delivery systems for Alzheimer's disease management: Technical, industrial, and clinical challenges. *J. Controlled Release 245*, 95−107.
(23) Maysinger, D., Groger, D., Lake, A., Licha, K., Weinhart, M., Chang, P. K., Mulvey, R., Haag, R., and McKinney, R. A. (2015) Dendritic polyglycerol sulfate inhibits microglial activation and reduces hippocampal CA1 dendritic spine morphology deficits. *Biomacromolecules 16*, 3073−3082.
(24) Cheng, C., Li, S., Thomas, A., Kotov, N. A., and Haag, R. (2017) Functional graphene nanomaterials based architectures: Biointeractions, fabrications, and emerging biological applications. *Chem. Rev. (Washington, DC, U. S.) 117*, 1826−1914.
(25) Haag, R., and Kratz, F. (2006) Polymer therapeutics: Concepts and applications. *Angew. Chem., Int. Ed. 45*, 1198−1215.
(26) Haag, R. (2004) Supramolecular drug-delivery systems based on polymeric core-shell architectures. *Angew. Chem., Int. Ed. 43*, 278−282.
(27) Stiriba, S. E., Frey, H., and Haag, R. (2002) Dendritic polymers in biomedical applications: From potential to clinical use in diagnostics and therapy. *Angew. Chem., Int. Ed. 41*, 1329−1334.
(28) Paulus, F., Schulze, R., Steinhilber, D., Zieringer, M., Steinke, I., Welker, P., Licha, K., Wedepohl, S., Dernedde, J., and Haag, R. (2014) The effect of polyglycerol sulfate branching on inflammatory processes. *Macromol. Biosci. 14*, 643−654.
(29) Pant, K., Groger, D., Bergmann, R., Pietzsch, J., Steinbach, J., Graham, B., Spiccia, L., Berthon, F., Czarny, B., Devel, L., Dive, V., Stephan, H., and Haag, R. (2015) Synthesis and biodistribution studies of (3)H- and (64)Cu-labeled dendritic polyglycerol and dendritic polyglycerol sulfate. *Bioconjugate Chem. 26*, 906−918.
(30) Licha, K., Welker, P., Weinhart, M., Wegner, N., Kern, S., Reichert, S., Gemeinhardt, I., Weissbach, C., Ebert, B., Haag, R., and Schirner, M. (2011) Fluorescence imaging with multifunctional polyglycerol sulfates: Novel polymeric near-IR probes targeting inflammation. *Bioconjugate Chem. 22*, 2453−2460.
(31) Groger, D., Paulus, F., Licha, K., Welker, P., Weinhart, M., Holzhausen, C., Mundhenk, L., Gruber, A. D., Abram, U., and Haag, R. (2013) Synthesis and biological evaluation of radio and dye labeled amino functionalized dendritic polyglycerol sulfates as multivalent anti-inflammatory compounds. *Bioconjugate Chem. 24*, 1507−1514.
(32) Chang, P. K., Khatchadourian, A., McKinney, R. A., and Maysinger, D. (2015) Docosahexaenoic acid (DHA): A modulator of microglia activity and dendritic spine morphology. *J. Neuroinflammation 12*, 34.
(33) Arbel-Ornath, M., Hudry, E., Boivin, J. R., Hashimoto, T., Takeda, S., Kuchibhotla, K. V., Hou, S., Lattarulo, C. R., Belcher, A. M., Shakerdge, N., Trujillo, P. B., Muzikansky, A., Betensky, R. A., Hyman, B. T., and Bacskai, B. J. (2017) Soluble oligomeric amyloid-beta induces calcium dyshomeostasis that precedes synapse loss in the living mouse brain. *Mol. Neurodegener. 12*, 27.
(34) Jung, C. K., and Herms, J. (2012) Role of APP for dendritic spine formation and stability. *Exp. Brain Res. 217*, 463−470.
(35) Lacor, P. N., Buniel, M. C., Furlow, P. W., Clemente, A. S., Velasco, P. T., Wood, M., Viola, K. L., and Klein, W. L. (2007) Abeta oligomer-induced aberrations in synapse composition, shape, and density provide a molecular basis for loss of connectivity in Alzheimer's disease. *J. Neurosci. 27*, 796−807.
(36) Laux, T., Fukami, K., Thelen, M., Golub, T., Frey, D., and Caroni, P. (2000) GAP43, MARCKS, and CAP23 modulate PI(4,5)P-2 at plasmalemmal rafts, and regulate cell cortex actin dynamics through a common mechanism. *J. Cell Biol. 149*, 1455−1471.
(37) Kim, S. K., Nabekura, J., and Koizumi, S. (2017) Astrocyte-mediated synapse remodeling in the pathological brain. *Glia 65*, 1719−1727.
(38) Perez-Alvarez, A., Navarrete, M., Covelo, A., Martin, E. D., and Araque, A. (2014) Structural and functional plasticity of astrocyte processes and dendritic spine interactions. *J. Neurosci. 34*, 12738−12744.
(39) Lindahl, U., and Li, J. P. (2009) Interactions between heparan sulfate and proteins-design and functional implications. *Int. Rev. Cell Mol. Biol. 276*, 105−159.
(40) Arungundram, S., Al-Mafraji, K., Asong, J., Leach, F. E., 3rd, Amster, I. J., Venot, A., Turnbull, J. E., and Boons, G. J. (2009) Modular synthesis of heparan sulfate oligosaccharides for structure-activity relationship studies. *J. Am. Chem. Soc. 131*, 17394−17405.
(41) Sadir, R., Imberty, A., Baleux, F., and Lortat-Jacob, H. (2004) Heparan sulfate/heparin oligosaccharides protect stromal cell-derived factor-1 (SDF-1)/CXCL12 against proteolysis induced by CD26/dipeptidyl peptidase IV. *J. Biol. Chem. 279*, 43854−43860.
(42) Nguyen, K., and Rabenstein, D. L. (2016) Interaction of the heparin-binding consensus sequence of beta-amyloid peptides with heparin and heparin-derived oligosaccharides. *J. Phys. Chem. B 120*, 2187−2197.
(43) Weinhart, M., Groger, D., Enders, S., Riese, S. B., Dernedde, J., Kainthan, R. K., Brooks, D. E., and Haag, R. (2011) The role of dimension in multivalent binding events: Structure-activity relationship of dendritic polyglycerol sulfate binding to L-selectin in correlation with size and surface charge density. *Macromol. Biosci. 11*, 1088−1098.
(44) Calamai, M., Kumita, J. R., Mifsud, J., Parrini, C., Ramazzotti, M., Ramponi, G., Taddei, N., Chiti, F., and Dobson, C. M. (2006) Nature and significance of the interactions between amyloid fibrils and biological polyelectrolytes. *Biochemistry 45*, 12806−12815.
(45) Qiang, W., Yau, W. M., Lu, J. X., Collinge, J., and Tycko, R. (2017) Structural variation in amyloid-beta fibrils from Alzheimer's disease clinical subtypes. *Nature 541*, 217−221.
(46) Harmeier, A., Wozny, C., Rost, B. R., Munter, L. M., Hua, H., Georgiev, O., Beyermann, M., Hildebrand, P. W., Weise, C., Schaffner, W., Schmitz, D., and Multhaup, G. (2009) Role of amyloid-beta glycine 33 in oligomerization, toxicity, and neuronal plasticity. *J. Neurosci. 29*, 7582−7590.
(47) Zhang, H., Su, Y. J., Zhou, W. W., Wang, S. W., Xu, P. X., Yu, X. L., and Liu, R. T. (2014) Activated scavenger receptor A promotes glial internalization of Abeta. *PLoS One 9*, e94197.
(48) Britt, D. J., Farias, G. G., Guardia, C. M., and Bonifacino, J. S. (2016) Mechanisms of polarized organelle distribution in neurons. *Front. Cell. Neurosci. 10*, 88.
(49) Pu, J., Guardia, C. M., Keren-Kaplan, T., and Bonifacino, J. S. (2016) Mechanisms and functions of lysosome positioning. *J. Cell Sci. 129*, 4329−4339.
(50) Vilchez, D., Saez, I., and Dillin, A. (2014) The role of protein clearance mechanisms in organismal ageing and age-related diseases. *Nat. Commun. 5*, 5659.
(51) Cuervo, A. M., and Macian, F. (2014) Autophagy and the immune function in aging. *Curr. Opin. Immunol. 29*, 97−104.
(52) Schneider, J. L., and Cuervo, A. M. (2014) Autophagy and human disease: Emerging themes. *Curr. Opin. Genet. Dev. 26*, 16−23.
(53) Ferreira, A. C., Da Mesquita, S., Sousa, J. C., Correia-Neves, M., Sousa, N., Palha, J. A., and Marques, F. (2015) From the periphery to the brain: Lipocalin-2, a friend or foe? *Prog. Neurobiol. (Oxford, U. K.) 131*, 120−136.
(54) Suk, K. (2016) Lipocalin-2 as a therapeutic target for brain injury: An astrocentric perspective. *Prog. Neurobiol. (Oxford, U. K.) 144*, 158−172.
(55) Mesquita, S. D., Ferreira, A. C., Falcao, A. M., Sousa, J. C., Oliveira, T. G., Correia-Neves, M., Sousa, N., Marques, F., and Palha, J.

DOI: 10.1021/acschemneuro.7b00301
ACS Chem. Neurosci. 2018, 9, 260−271

A. (2014) Lipocalin 2 modulates the cellular response to amyloid beta. *Cell Death Differ. 21*, 1588−1599.
(56) Mucha, M., Skrzypiec, A. E., Schiavon, E., Attwood, B. K., Kucerova, E., and Pawlak, R. (2011) Lipocalin-2 controls neuronal excitability and anxiety by regulating dendritic spine formation and maturation. *Proc. Natl. Acad. Sci. U. S. A. 108*, 18436−18441.
(57) Lee, S., Kim, J. H., Kim, J. H., Seo, J. W., Han, H. S., Lee, W. H., Mori, K., Nakao, K., Barasch, J., and Suk, K. (2011) Lipocalin-2 is a chemokine inducer in the central nervous system role of chemokine ligand 10 (CXCL10) in lipocalin-2-induced cell migration. *J. Biol. Chem. 286*, 43855−43870.
(58) Bi, F., Huang, C., Tong, J., Qiu, G., Huang, B., Wu, Q., Li, F., Xu, Z., Bowser, R., Xia, X. G., and Zhou, H. (2013) Reactive astrocytes secrete lcn2 to promote neuron death. *Proc. Natl. Acad. Sci. U. S. A. 110*, 4069−4074.
(59) Lee, S., Jha, M. K., and Suk, K. (2015) Lipocalin-2 in the inflammatory activation of brain astrocytes. *Crit. Rev. Immunol. 35*, 77−84.
(60) Dekens, D. W., Naude, P. J., Engelborghs, S., Vermeiren, Y., Van Dam, D., Oude Voshaar, R. C., Eisel, U. L., and De Deyn, P. P. (2017) Neutrophil gelatinase-associated lipocalin and its receptors in Alzheimer's disease (AD) brain regions: Differential findings in AD with and without depression. *J. Alzheimer's Dis. 55*, 763−776.
(61) Garwood, C. J., Pooler, A. M., Atherton, J., Hanger, D. P., and Noble, W. (2011) Astrocytes are important mediators of Abeta-induced neurotoxicity and tau phosphorylation in primary culture. *Cell Death Dis. 2*, e167.
(62) Finnema, S. J., Nabulsi, N. B., Eid, T., Detyniecki, K., Lin, S. F., Chen, M. K., Dhaher, R., Matuskey, D., Baum, E., Holden, D., Spencer, D. D., Mercier, J., Hannestad, J., Huang, Y., and Carson, R. E. (2016) Imaging synaptic density in the living human brain. *Sci. Transl. Med. 8*, 348ra96.
(63) Türk, H., Shukla, A., Alves Rodrigues, P. C., Rehage, H., and Haag, R. (2007) Water-soluble dendritic core-shell-type architectures based on polyglycerol for solubilization of hydrophobic drugs. *Chem. - Eur. J. 13*, 4187−4196.
(64) Roher, A. E., Chaney, M. O., Kuo, Y. M., Webster, S. D., Stine, W. B., Haverkamp, L. J., Woods, A. S., Cotter, R. J., Tuohy, J. M., Krafft, G. A., Bonnell, B. S., and Emmerling, M. R. (1996) Morphology and toxicity of Abeta-(1−42) dimer derived from neuritic and vascular amyloid deposits of Alzheimer's disease. *J. Biol. Chem. 271*, 20631−20635.
(65) Schmechel, A., Zentgraf, H., Scheuermann, S., Fritz, G., Pipkorn, R., Reed, J., Beyreuther, K., Bayer, T. A., and Multhaup, G. (2003) Alzheimer beta-amyloid homodimers facilitate A beta fibrillization and the generation of conformational antibodies. *J. Biol. Chem. 278*, 35317−35324.
(66) Gahwiler, B. H., Capogna, M., Debanne, D., McKinney, R. A., and Thompson, S. M. (1997) Organotypic slice cultures: a technique has come of age. *Trends Neurosci. 20*, 471−477.
(67) Richards, D. A., Mateos, J. M., Hugel, S., de Paola, V., Caroni, P., Gahwiler, B. H., and McKinney, R. A. (2005) Glutamate induces the rapid formation of spine head protrusions in hippocampal slice cultures. *Proc. Natl. Acad. Sci. U. S. A. 102*, 6166−6171.
(68) Myszka, D. G. (1999) Improving biosensor analysis. *J. Mol. Recognit. 12*, 279−284.

DOI: 10.1021/acschemneuro.7b00301
ACS Chem. Neurosci. 2018, 9, 260−271